A FAST SOLVER FOR A NONLOCAL DIELECTRIC CONTINUUM MODEL*

DEXUAN XIE†, YI JIANG†, PETER BRUNE‡, AND L. RIDGWAY SCOTT‡

Abstract. The nonlocal continuum dielectric model is an important extension of the classical Poisson dielectric model, but it is very expensive to be solved in general. In this paper, we prove that the solution of one commonly used nonlocal continuum dielectric model of water can be split as a sum of two functions, and these two functions are simply the solutions of one Poisson equation and one Poisson-like equation. With this new solution splitting formula, we develop a fast finite element algorithm and a program package in Python based on the `DOLFIN` program library such that a nonlocal dielectric model can be solved numerically in an amount of computation that merely doubles that of solving a classic Poisson dielectric model. Using the new solution splitting formula, we also derive the analytical solutions of two nonlocal model problems. We then solve these two nonlocal model problems numerically by our program package and validate the numerical solutions through a comparison with the analytical solutions. Finally, our study of free energy calculation by a nonlocal Born ion model demonstrates that the nonlocal dielectric model is a much better predictor of the solvation free energy of ions than the local Poisson dielectric model.

Key words. Nonlocal dielectric continuum model, Poisson equation, electrostatic potential, finite element method

AMS subject classifications. 92-08 65N30

1. Introduction. The nonlocal dielectric approach for estimating electrostatics was investigated by Dogonadze and Kornyshev (see [6, 13, 20]) about 30 years ago. Since then, many studies have been done in the fields of chemistry, physics, and biology (see [5, 6, 7, 8, 20, 21, 26, 28], for example). A good review on these studies is given in [4]. The model is appropriate for a wide range of dielectric materials, certainly for any dipolar liquid in particular. In a nonlocal continuum solvent model, the water is treated as a dielectric medium with a dielectric permittivity function nonzero over the whole space in order to reflect the electrostatic solute-solvent interactions, the finite-size effects of the dielectric water molecules, and the spatial-frequency dependence of the dielectric permittivity. It has been recognized that a nonlocal continuum solvent model can significantly improve the quality of the classic Poisson model in electrostatic modeling [11, 25, 26]. However, because its nonlocal term involves a convolution of the electric field over the whole space, a nonlocal dielectric model becomes very expensive to be solved numerically. The absence of efficient numerical algorithms and software packages has seriously restricted its application in large scale biomolecular simulations.

Remarkable progress in the development of fast numerical algorithms was made by Hildebrandt *et al.*[18] when they reformulated one commonly used nonlocal electrostatic continuum model, called the Fourier-Lorentzian nonlocal model, as a system of coupled partial differential equations. The details of this reformulation and a related boundary element algorithm are also given in Hildebrant's dissertation [17]. Recently, a finite difference implementation of the nonlocal dielectric model has been given [29].

Motivated by the work of Hildebrandt *et al.*, we propose a new formulation of the nonlocal dielectric model. A key step is to write the nonlocal dielectric model as an integro-differential equation in which the integral term involves only a convolution

*This work was partially supported by National Science Foundation, USA, grant DMS-0921004.

†Department of Mathematical Sciences. University of Wisconsin-Milwaukee, Milwaukee, Wisconsin, USA, 53201-0413 (`dxie@uwm.edu`)

‡ Department of Computer Science, University of Chicago, Chicago, IL 60637

of the electrostatic potential function $\Phi(\mathbf{r})$. The convolution of Φ is then regarded as a unknown function, $u(\mathbf{r})$. To calculate $u(\mathbf{r})$, we construct an "artificial" partial differential equation and couple this equation with the original equation of the nonlocal dielectric model, yielding a system of two partial differential equations for solving both u and Φ. This approach can be naturally carried out in the framework of the Ritz-Galerkin variational formulation without involving any Helmholtz decomposition of the dielectric displacement field. Hence, it is quite different from the approach of Hildebrandt *et al.*[18]. Our approach works as long as the kernel in the nonlocal model corresponds to the inverse of a differential operator, as in (2.8). Its difference from the approach of Hildebrandt *et al.*'s [18] can best be seen by comparing our reformulation with equation (10) in [29], which involves a different splitting and the inclusion of jump terms.

Based on our new approach, we prove that the solution $\Phi(\mathbf{r})$ of the nonlocal dielectric model can be split as a sum of two functions, and these two functions are simply the solutions of one Poisson equation and one Poisson-like equation each suitable for solution by a fast linear solver such as the multigrid method [14]. As an application of this solution splitting formula, we derive the analytical solutions of two nonlocal dielectric models: one with one point charge, and the other with a smooth charge density function. We then develop a finite element algorithm and program it into a computer package in Python based on the finite element program library `DOLFIN` [22]. Because of this program package, we can solve the nonlocal dielectric model by using various finite element approximations from `DOLFIN` and various efficient direct and iterative linear solvers from the `PETSc` library [2, 3], the UMFPACK library [12], and the Trilinos project [16]. Since it is programed in Python, this program package is easy to use. It is also portable on different computer operating systems and can be implemented in parallel on a parallel computer or a cluster. Therefore, this program package can be a powerful tool for solving a large scale nonlocal dielectric model numerically.

To validate our new solution split formula and our program package, we made numerical experiments using the two nonlocal model problems whose analytical solutions we derived by the new solution split formula. Numerical results show that the numerical solutions match the analytical solutions very well, which well confirm the solution split formula and validate the program package. In these tests, each linear system was solved by the preconditioned conjugate gradient (PCG) method with incomplete LU (ILU) preconditioning from `PETSc` (with the relative residue less than 10^{-10}). We also made tests using an algebraic multigrid preconditioner, called *amg_hypre*, from `PETSc`, which was found to cost more CPU time than ILU in spite of a sharp reduction of the total number of PCG iterations. It appears from our data that our problem size is not large enough for multigrid efficiency to be needed. Indeed our setup times dominate our solve times.

Finally, using the analytical expression of the free energy of a nonlocal Born ion model, which we derive in the appendix, we calculated the free energy for nine different types of ions and found that the free energy calculated from the nonlocal dielectric model can match very well the one produced from chemical experiments by using a properly selected value of a parameter of the nonlocal dielectric model that is used to characterize the polarization correlations of water molecules. This study of free energy calculation demonstrates that the nonlocal dielectric model is a much better predictor of the solvation free energy of ions than the classic Poisson dielectric model.

In the future, we will extend our fast solver to the case of a protein immersed

in water, which was studied in [29]. In such a case, a cavity domain hosting the protein is treated as another continuum dielectric medium such that the nonlocal model becomes an interface problem. Furthermore, we will consider an ionic solvent. Like what is done in the formulation of the Poisson-Boltzmann equation [19, 23], a nonlinear term will be introduced to estimate the distributions of ions so that the nonlocal model is modified as a nonlinear problem. We plan to use the same solution splitting techniques as those used in this paper to develop a new fast algorithm for solving these kinds of nonlocal and nonlinear dielectric continuum models.

The paper is organized as follows. Section 2 introduces a new expression of the Fourier-Lorentzian nonlocal dielectric model, and discusses the free energy calculations. Section 3 studies the computational complexity of solving the nonlocal model. Section 4 proves the new solution splitting formula. Section 5 derives the analytical solutions of the two nonlocal model problems. Section 6 presents the fast finite element algorithm. Section 7 describes the program package and reports numerical results. The free energy calculation and the analytical solution of a nonlocal Born ion model are reported in the appendix.

2. Fourier-Lorentzian nonlocal model of water and free energy calculations. Let $\Phi(\mathbf{r})$ denote the electrostatic potential function, and let $\rho(\mathbf{r})$ be a given fixed charge density function in the whole space $\mathbb{R}^3$. One commonly used nonlocal dielectric model, called the Fourier-Lorentzian nonlocal model, is defined by the integro-differential equation

$$\begin{cases} -\epsilon_0 \left[\epsilon_\infty \Delta\Phi(\mathbf{r}) + \frac{\epsilon_s-\epsilon_\infty}{\lambda^2}\nabla\cdot\int_{\mathbb{R}^3} H(\mathbf{r}-\mathbf{r}')\nabla\Phi(\mathbf{r}')\,\mathrm{d}\mathbf{r}'\right] = \rho(\mathbf{r}), & \mathbf{r}\in\mathbb{R}^3, \\ \Phi(\mathbf{r}) \to 0 & \text{as } |\mathbf{r}|\to\infty, \end{cases} \tag{2.1}$$

where ϵ_0 is the permittivity constant of the vacuum, ϵ_s is the permittivity factor for bulk water, $H(\mathbf{r})$ is the kernel function defined by

$$H(\mathbf{r}) = \frac{1}{4\pi|\mathbf{r}|}e^{-|\mathbf{r}|/\lambda}, \tag{2.2}$$

$\nabla = \left(\frac{\partial}{\partial x}, \frac{\partial}{\partial y}, \frac{\partial}{\partial z}\right)$ is the gradient operator and $\Delta = \frac{\partial^2}{\partial x^2} + \frac{\partial^2}{\partial y^2} + \frac{\partial^2}{\partial z^2}$ is the Laplace operator for $\mathbf{r} = (x, y, z)$, λ is a positive parameter used to characterize the polarization correlations of water molecules, and ϵ_∞ is the permittivity factor for water in the limit of high frequency [30]. This limit is also approached in the nonlocal model as $\lambda \to \infty$ [18]. Physically, ϵ_∞ accounts for the polarization of the electron density of individual water molecules, whereas ϵ_s represents the combination of this effect with rotations of the waters. Usually, we have that $\epsilon_\infty < \epsilon_s$. As a special case, if $\epsilon_\infty = \epsilon_s$, the nonlocal model is reduced to the classic Poisson dielectric model:

$$\begin{cases} -\epsilon_0\epsilon_s\Delta\Phi(\mathbf{r}) = \rho(\mathbf{r}), & \mathbf{r}\in\mathbb{R}^3, \\ \Phi(\mathbf{r}) \to 0 & \text{as } |\mathbf{r}|\to\infty. \end{cases} \tag{2.3}$$

2.1. Application in free energy calculations. One important application of the nonlocal model is to calculate the solvent free energy, which is a physical quantity of interest, that is, the free energy associated with moving the charged system from the vacuum into the solvent (water). A common estimate of this is given simply by the electrostatic energy

$$\int_{\mathbb{R}^3} \Phi(\mathbf{r})\rho(\mathbf{r})\,d\mathbf{r}. \tag{2.4}$$

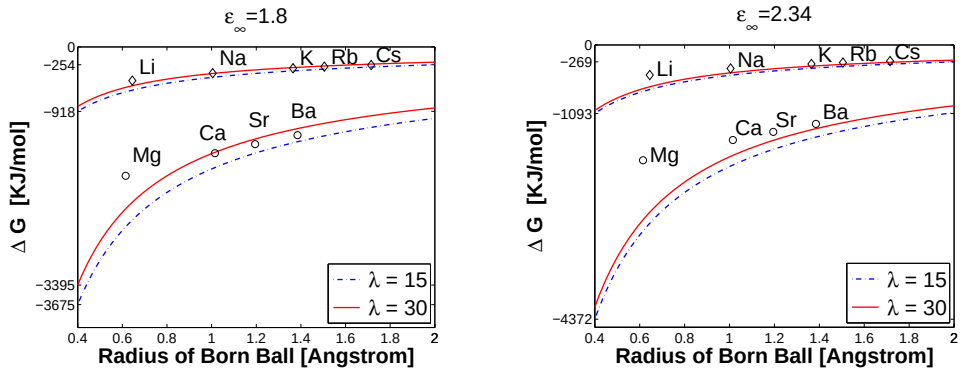

FIG. 2.1. *Comparisons of analytical free energy differences calculated from the nonlocal dielectric model with two values of λ and the values from chemical experiments (Table 5.10 on page 107 in [24]), for 9 different types of ions, with $\epsilon_\infty = 1.8$ [17] and $\epsilon_\infty = 2.34$ [31].*

To illustrate the great potential of the nonlocal model in this application, we consider the free energy G, in units of kilojoules per mole, of the Born ion model, which can be estimated as follows:

$$G \approx \frac{\mathcal{N}_a}{1000}\frac{1}{2}\int_{\mathbb{R}^3} \Phi(\mathbf{r})\rho(\mathbf{r})\,\mathrm{d}\mathbf{r}, \tag{2.5}$$

where $\mathcal{N}_a$ is the Avogadro constant. We note that the point charge model for an ion (i.e., $\rho = q\delta$ with q being a charge and δ the Dirac-delta distribution) is not appropriate to estimate its solvent free energy, since the only energy that would appear is the self-energy (2.4), which is infinite. However, the Born model replaces the point charge by a distributed charge, making it possible to define a solvent free energy in this case, for which (2.4) is finite and meaningful. In the appendix, we derive the analytical solutions of a nonlocal Born ion model (see (.11)) and the local Poisson dielectric model in both vacuum and water states (see (.12)). The free energy difference between the solvated state and the vacuum state is then found as follows:

$$\Delta G \approx \begin{cases} \frac{\mathcal{N}_a}{1000} C \left[\frac{\sqrt{\frac{\epsilon_\infty}{\epsilon_s}} + \coth\frac{a}{\lambda}}{\sqrt{\frac{\epsilon_\infty}{\epsilon_s}} + \frac{\lambda}{a}\left(\frac{\epsilon_\infty}{\epsilon_s} - 1\right) + \coth\frac{a}{\lambda}} - \epsilon_s \right] & \text{for nonlocal Born ion model,} \\ \frac{\mathcal{N}_a}{1000} C \left(1 - \epsilon_s\right) & \text{for local Born ion model,} \end{cases} \tag{2.6}$$

where $C = q^2/(8\pi\epsilon_0\epsilon_s a)$, a denotes the radius of the Born ball $B_a = \{\mathbf{r} \mid |\mathbf{r}| < a\}$, and q is the charge of an ion at the origin, which has been spread over the spheric surface of B_a. From the above expression we can see that the free energy ΔG can be regarded as a function of parameter λ in the case of the nonlocal dielectric model, where $0 < \lambda < \infty$, and can be reduced to the case of the Poisson local model with the permittivity constants being ϵ_s and ϵ_∞, respectively, as $\lambda \to 0$ and $\lambda \to \infty$.

With (2.6) and the data from Tables 2.1 and 2.2, we calculated the free energy differences for the nine different types of ions indicated in Figure 2.1. We also show the results for two ions as a function of the parameter λ in Figure 2.2. We see that the nonlocal model provides fairly accurate predictions and goes from the classic Poisson model when $\lambda = 0$ to a limiting case for large λ. Fortuitous values of λ that match the experimental values exactly are given as a guide. Table 2.2 gives data on the free energies and atomic radii from experiments. Results for the Born ion model for two values of λ that bracket the value $\lambda = 23$Å used in [17] are shown in Figure

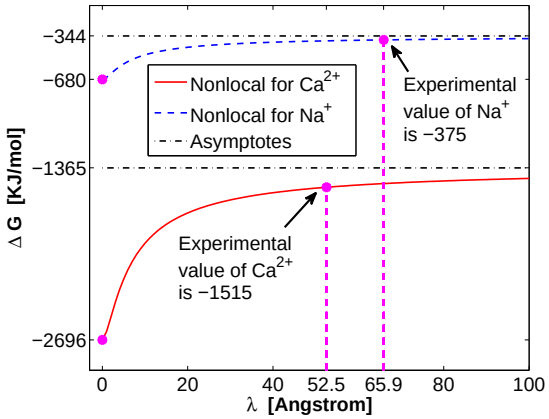

FIG. 2.2. *Comparisons of analytical free energy differences calculated from the nonlocal dielectric model ($\epsilon_\infty = 2$) with the ones produced from chemical experiments and the classic Poisson dielectric model for ions Ca^{2+} (with $q = +2e$) and Na^{+} (with $q = +1e$). The values for $\lambda = 0$ correspond to the classic local Poisson dielectric model.*

2.1. The predicted results are remarkably accurate for most ions, especially given the uncertainty in the ion radius as shown in Table 2.2. Moreover, it is relatively insensitive to the choice of λ. We should note that we are accounting only for the polar contribution to the free energy, and that there is a nonpolar part that must also be estimated [17]. Hence, the nonlocal dielectric model is a much better predictor of the solvation free energy of ions than the classic Poisson dielectric model.

TABLE 2.1
Physics parameter values used for computing free energy differences

Constant	Definition	Value
$\mathcal{N}_a$	Avogadro constant	6.022×10^{23}/mole
ϵ_s	permittivity ratio of bulk water	80 [15]
ϵ_∞	limit permittivity ratio	1.8 [17], 2.34 [31]
ϵ_0	permittivity of vacuum	8.854×10^{-12} Farad/meter
$1e$	one electron charge	1.6×10^{-19} Coulomb

TABLE 2.2
Free energy differences produced from chemical experiments for selected ions, together with the atomic radii and their uncertainties [17].

Ion	Radius of Born ball [Å]	Charge [e]	Free energy [KJ/mol]
Na^+	1.005 ± 0.04	1	-375
K^+	1.365 ± 0.05	1	-304
Ca^{2+}	1.015 ± 0.02	2	-1515
Sr^{2+}	1.195	2	-1386

Remark 1: Although there are a lot of constants in (2.6), almost all of them are physical constants. The only parameters being estimated in these models are the Born radius a and the nonlocal dielectric modulation parameter λ. Note that the

ratio a/λ is dimensionless. The coefficient ϵ_s is a measured permittivity ratio of bulk water, appropriate at a temperature $T \approx 20.3$ degrees Celsius [15], and the coefficient ϵ_∞ is an estimated permittivity ratio of confined water. In [17], a value $\epsilon_\infty = 1.8$ was used. The resulting energy estimates are very sensitive to the exact value of parameter ϵ_∞. For example, we illustrate in Figure 2.1 the energies predicted using a value of $\epsilon_\infty = 2.34$ [31]. We note that even higher values of ϵ_∞ are seen experimentally (at lower temperatures) in various forms of ice [30].

2.2. A new expression of the nonlocal model. However, it is usually very expensive and very difficult to solve a nonlocal dielectric model. The main difficulty in solving the nonlocal model (2.1) comes from the integral term in which the integration and derivative are mixed together. To overcome this difficulty, we start to simplify this integral term using the following property of convolution [27]:

Differential Property of Convolution. If the convolution $v * H$ is defined by

$$(v * H)(\mathbf{r}) = \int_{\mathbb{R}^3} v(\mathbf{r}')H(\mathbf{r} - \mathbf{r}')\,\mathrm{d}\mathbf{r}' \quad \forall \mathbf{r} \in \mathbb{R}^3,$$

then its $|\alpha|$th derivative $D^\alpha(v * H)$ has the property

$$D^\alpha(v * H) = (D^\alpha v) * H = v * D^\alpha H, \tag{2.7}$$

where $D^\alpha = (\partial/\partial x)^{\alpha_1}(\partial/\partial y)^{\alpha_2}(\partial/\partial z)^{\alpha_3}$, $\alpha = (\alpha_1, \alpha_2, \alpha_3)$ with α_1, α_2, and α_3 being nonnegative integers, and $|\alpha| = \alpha_1 + \alpha_2 + \alpha_3$.

According to the above property, it is straightforward to get that

$$\nabla\cdot \int_{\mathbb{R}^3} H(\mathbf{r} - \mathbf{r}')\nabla\Phi(\mathbf{r}')\,\mathrm{d}\mathbf{r}' = (\Phi * \Delta H)(\mathbf{r}), \quad \mathbf{r} \in \mathbb{R}^3.$$

Note that $H(\mathbf{r})$ satisfies the following equation:

$$-\Delta H + \frac{1}{\lambda^2} H = \delta, \tag{2.8}$$

where δ is the Dirac-delta distribution defined by $\delta(f) = f(0)$ for any test function f [27]. Hence, applying the convolution on the both sides of (2.8) gives

$$(\Phi * \Delta H)(\mathbf{r}) = \frac{1}{\lambda^2}(\Phi * H)(\mathbf{r}) - \Phi(\mathbf{r}), \quad \mathbf{r} \in \mathbb{R}^3. \tag{2.9}$$

As a result, the integral term in (2.1) is simplified as

$$\nabla\cdot \int_{\mathbb{R}^3} H(\mathbf{r} - \mathbf{r}')\nabla\Phi(\mathbf{r}')\,\mathrm{d}\mathbf{r}' = \frac{1}{\lambda^2}(\Phi * H)(\mathbf{r}) - \Phi(\mathbf{r}), \quad \mathbf{r} \in \mathbb{R}^3,$$

so that the nonlocal model (2.1) is reformulated into the new expression

$$-\epsilon_\infty \Delta\Phi(\mathbf{r}) + \frac{\epsilon_s - \epsilon_\infty}{\lambda^2}\Phi(\mathbf{r}) - \frac{\epsilon_s - \epsilon_\infty}{\lambda^4}(\Phi * H)(\mathbf{r}) = \frac{1}{\epsilon_0}\rho(\mathbf{r}), \quad \mathbf{r} \in \mathbb{R}^3. \tag{2.10}$$

3. Complexity of the Fourier-Lorenztian model. Equation (2.10) disentangles the derivatives and integral operator in the original equation (2.1). Even so, it is still very expensive to solve. To illustrate this, we consider a finite element approximation of (2.10) in the following.

For simplicity, a sufficiently large spherical domain, Ω, is selected to set up the Dirichlet boundary condition $\Phi = 0$ on the boundary $\partial\Omega$ of Ω, and we extend Φ by zero outside this domain. Thus, (2.10) is approximated as the following boundary value problem:

$$\begin{cases} -\epsilon_\infty \Delta\Phi(\mathbf{r}) + \frac{\epsilon_s-\epsilon_\infty}{\lambda^2}\Phi(\mathbf{r}) - \frac{\epsilon_s-\epsilon_\infty}{\lambda^4}(\Phi * H)(\mathbf{r}) = \frac{1}{\epsilon_0}\rho(\mathbf{r}), & \mathbf{r}\in\Omega, \\ \Phi(\mathbf{r}) = 0 & \text{on } \partial\Omega. \end{cases} \tag{3.1}$$

We then formulate (3.1) in the following variational form.

Find $\Phi \in H_0^1(\Omega)$ such that

$$a(\Phi,\, \psi) = l(\psi) \quad \forall \psi \in H_0^1(\Omega), \tag{3.2}$$

where $H_0^1(\Omega)$ denotes the Sobolev function space defined by

$$H_0^1(\Omega) = \{\psi \mid \|D^\alpha \psi\|_{L^2(\Omega)} < \infty \quad \forall |\alpha| \le 1, \text{ and } \psi|_{\partial\Omega} = 0\},$$

$a(\Phi, \psi)$ is a bilinear functional defined by

$$a(\Phi,\psi) = \epsilon_\infty \int_\Omega \nabla\Phi\cdot\nabla\psi \; dr + \frac{\epsilon_s-\epsilon_\infty}{\lambda^2}\int_\Omega \Phi\psi \,\mathrm{d}\mathbf{r} - \frac{\epsilon_s-\epsilon_\infty}{\lambda^4}\int_\Omega u(\mathbf{r})\psi(\mathbf{r})\,\mathrm{d}\mathbf{r}, \tag{3.3}$$

and $l(\psi)$ is a linear functional defined by

$$l(\psi) = \frac{1}{\epsilon_0}\int_\Omega \rho(\mathbf{r})\psi(\mathbf{r})\,\mathrm{d}\mathbf{r}. \tag{3.4}$$

Here we have denoted the convolution term as a function

$$u(\mathbf{r}) = (\Phi * H)(\mathbf{r}) \quad \forall \mathbf{r}\in\mathbb{R}^3. \tag{3.5}$$

We next show that the finite element approximation to the above variational problem results in a fully dense linear system.

To solve (3.2) by the finite element method, we consider a confirming finite element space $\mathcal{V}_h$, which is constructed based on a triangulation (partition into tetrahedra) $\mathcal{T}_h$ of Ω with a mesh size of h such that $\mathcal{V}_h \subset H_0^1(\Omega)$. Let $\{\varphi_j\}_{j=1}^N$ be a set of N basis functions of $\mathcal{V}_h$, which satisfies

$$\varphi_j(\mathbf{r}_i) = \begin{cases} 1, & i = j, \\ 0, & i \ne j, \end{cases} \qquad \text{for } i,j = 1,2,\ldots,N, \tag{3.6}$$

where N is the total number of the interior mesh points of the triangulation $\mathcal{T}_h$, $\mathbf{r}_i$ is the ith internal vertex of $\mathcal{T}_h$, and φ_j is a linear function on each tetrahedral element of $\mathcal{T}_h$. Thus, for $\Phi_h \in \mathcal{V}_h$,

$$\Phi_h(\mathbf{r}) = \sum_{j=1}^N \Phi_j\varphi_j(\mathbf{r}), \quad \mathbf{r}\in\Omega, \tag{3.7}$$

where Φ_j is a numerical approximation to $\Phi(\mathbf{r}_j)$ for $\Phi \in H_0^1(\Omega)$. The variational problem (3.2) is then approximated as the following finite element equation.

Find Φ_h in the form (3.7) such that

$$\sum_{i=1}^N a(\varphi_i,\varphi_j)\Phi_i = l(\varphi_j), \quad j = 1,2,\ldots,N. \tag{3.8}$$

Clearly, the above system of linear equations can be written in the matrix form

$$Ax = b, \tag{3.9}$$

where $x = (\Phi_1, \Phi_2, \ldots, \Phi_N)^T$, $b = (l(\varphi_1), l(\varphi_2), \ldots, l(\varphi_N))^T$, and A is an $N \times N$ matrix with $a(\varphi_i,\, \varphi_j)$ as the (j,i)th entry.

Each entry $a(\varphi_i,\, \varphi_j)$ of matrix A contains the term $\int_\Omega \widetilde{\varphi}_i(\mathbf{r})\varphi_j(\mathbf{r})\,\mathrm{d}\mathbf{r}$, where $\widetilde{\varphi}_i$ denotes the convolution of φ_i; for any $\mathbf{r} \in \Omega$, we have

$$\widetilde{\varphi}_i(\mathbf{r}) = \int_\Omega H(\mathbf{r}-\mathbf{r}')\varphi_i(\mathbf{r}')\,\mathrm{d}\mathbf{r}' = \int_{\omega_i} H(\mathbf{r}-\mathbf{r}')\varphi_i(\mathbf{r}')\,\mathrm{d}\mathbf{r}',$$

where ω_i denotes the support of $\varphi_i(\mathbf{r})$. Since φ_i is positive in the interior of ω_i and $H > 0$ everywhere, the support of $\widetilde{\varphi}_i$ is the whole domain. Hence, we have that

$$\int_\Omega \widetilde{\varphi}_i(\mathbf{r})\varphi_j(\mathbf{r})\,\mathrm{d}\mathbf{r} = \int_{\omega_j} \widetilde{\varphi}_i(\mathbf{r})\varphi_j(\mathbf{r})\,\mathrm{d}\mathbf{r} \neq 0 \quad \text{for } i,j = 1,2,\ldots,N.$$

Consequently, $a(\varphi_i, \varphi_j) \neq 0$ for all $i, j = 1, 2, \ldots, N$. This completes the proof that A is a fully dense matrix. Therefore, it is too expensive to solve the linear system (3.9) for a large value of N. Further reformulation is needed to derive a fast numerical solver.

4. New solution splitting formula. In this section, we show that the solution $\Phi(\mathbf{r})$ of the nonlocal model (2.1) can be split as a sum of two functions, and the two functions are simply the solutions of one Poisson equation and one Poisson-like equation. For clarity, we present this solution splitting formula in the following theorem.

THEOREM 4.1. *Let Φ be the solution of the nonlocal model* (2.1)*. Then it can be expressed as*

$$\Phi(\mathbf{r}) = \frac{1}{\lambda^2\epsilon_s}[(\epsilon_s - \epsilon_\infty)w(\mathbf{r}) + \epsilon_\infty v(\mathbf{r})], \quad \mathbf{r} \in \mathbb{R}^3, \tag{4.1}$$

where $w(\mathbf{r})$ is the solution of the Poisson-like equation

$$\begin{cases} -\Delta w(\mathbf{r}) + \dfrac{\epsilon_s}{\lambda^2\epsilon_\infty} w(\mathbf{r}) = \dfrac{\lambda^2}{\epsilon_0\epsilon_\infty}\rho(\mathbf{r}), \quad \mathbf{r} \in \mathbb{R}^3, \\ \qquad\qquad w(\mathbf{r}) \to 0 \qquad \text{as } |\mathbf{r}| \to \infty, \end{cases} \tag{4.2}$$

and $v(\mathbf{r})$ is the solution of the Poisson equation

$$\begin{cases} -\Delta v(\mathbf{r}) = \dfrac{\lambda^2}{\epsilon_0\epsilon_\infty}\rho(\mathbf{r}), \quad \mathbf{r} \in \mathbb{R}^3, \\ \qquad v(\mathbf{r}) \to 0 \qquad \text{as } |\mathbf{r}| \to \infty. \end{cases} \tag{4.3}$$

Proof. Using (2.7) and the notation of u given in (3.5), we can easily reformulate (2.9) as an equation for determining u:

$$-\Delta u(\mathbf{r}) + \frac{1}{\lambda^2} u(\mathbf{r}) = \Phi(\mathbf{r}) \quad \forall \mathbf{r} \in \mathbb{R}^3. \tag{4.4}$$

We then couple (4.4) with (2.10) to yield a system for solving both Φ and u:

$$\begin{cases} -\epsilon_\infty \Delta\Phi(\mathbf{r}) + \dfrac{\epsilon_s - \epsilon_\infty}{\lambda^2}\Phi(\mathbf{r}) - \dfrac{\epsilon_s - \epsilon_\infty}{\lambda^4}u(\mathbf{r}) = \dfrac{1}{\epsilon_0}\rho(\mathbf{r}), \\ -\Delta u(\mathbf{r}) + \dfrac{1}{\lambda^2}u(\mathbf{r}) - \Phi(\mathbf{r}) = 0, \end{cases} \tag{4.5}$$

where $\mathbf{r} \in \mathbb{R}^3$, and both $\Phi(\mathbf{r})$ and $u(\mathbf{r})$ approach zero as $|\mathbf{r}| \to \infty$.

From the second equation of (4.5) we can get

$$\Phi = \frac{1}{\lambda^2}(-\lambda^2\Delta u + u) = \frac{1}{\lambda^2}(w + u), \tag{4.6}$$

provided that w is set by

$$w(\mathbf{r}) = -\lambda^2\Delta u(\mathbf{r}) \quad \forall \mathbf{r} \in \mathbb{R}^3. \tag{4.7}$$

Clearly, if w is given, (4.7) can be rewritten as the equation for determining u:

$$-\Delta u(\mathbf{r}) = \frac{1}{\lambda^2}w(\mathbf{r}) \quad \forall \mathbf{r} \in \mathbb{R}^3. \tag{4.8}$$

Thus, the key issue is how to find an equation for determining w. To do so, we multiply $\frac{\lambda^4}{\epsilon_s - \epsilon_\infty}$ on the both sides of the first equation of (4.5) to get

$$\left(-\frac{\lambda^4\epsilon_\infty}{\epsilon_s - \epsilon_\infty}\Delta + \lambda^2\right)\Phi - u = \frac{\lambda^4}{\epsilon_0(\epsilon_s - \epsilon_\infty)}\rho.$$

By substituting the function Φ with the expression of (4.6), the left-hand side of the above equation can be reformulated as

$$\begin{aligned} &\left(-\frac{\lambda^4\epsilon_\infty}{\epsilon_s - \epsilon_\infty}\Delta + \lambda^2\right)\Phi - u \\ =&\left(-\frac{\lambda^4\epsilon_\infty}{\epsilon_s - \epsilon_\infty}\Delta + \lambda^2\right)\frac{w + u}{\lambda^2} - u \\ =&\left(-\frac{\lambda^2\epsilon_\infty}{\epsilon_s - \epsilon_\infty}\Delta + 1\right)w + \left(-\frac{\lambda^2\epsilon_\infty}{\epsilon_s - \epsilon_\infty}\Delta + 1\right)u - u \\ =&\left(-\frac{\lambda^2\epsilon_\infty}{\epsilon_s - \epsilon_\infty}\Delta + 1\right)w - \frac{\lambda^2\epsilon_\infty}{\epsilon_s - \epsilon_\infty}\Delta u. \end{aligned}$$

Thus, the first equation of (4.5) becomes

$$\left(-\frac{\lambda^2\epsilon_\infty}{\epsilon_s - \epsilon_\infty}\Delta + 1\right)w - \frac{\lambda^2\epsilon_\infty}{\epsilon_s - \epsilon_\infty}\Delta u = \frac{\lambda^4}{\epsilon_0(\epsilon_s - \epsilon_\infty)}\rho$$

or, equivalently,

$$-\lambda^2\epsilon_\infty\Delta w + \epsilon_s w - \epsilon_\infty(w + \lambda^2\Delta u) = \frac{\lambda^4}{\epsilon_0}\rho.$$

Because of (4.7), the above equation is simplified into (4.2).

We next show how to get (4.3). By (4.7), the following equation is followed from (4.2):

$$-\Delta w(\mathbf{r}) + \frac{\epsilon_s}{\lambda^2\epsilon_\infty}(-\lambda^2\Delta u(\mathbf{r})) = \frac{\lambda^2}{\epsilon_0\epsilon_\infty}\rho(\mathbf{r}), \quad \mathbf{r}\in\mathbb{R}^3,$$

which can be simplified as

$$-\Delta\left(w(\mathbf{r}) + \frac{\epsilon_s}{\epsilon_\infty}u(\mathbf{r})\right) = \frac{\lambda^2}{\epsilon_0\epsilon_\infty}\rho(\mathbf{r}), \quad \mathbf{r}\in\mathbb{R}^3.$$

We then obtain (4.3) by setting

$$v = w + \frac{\epsilon_s}{\epsilon_\infty}u. \tag{4.9}$$

When v is given, we solve the above equation for u to get

$$u = \frac{\epsilon_\infty}{\epsilon_s}(v - w)$$

so that from (4.6) it implies the solution splitting formula (4.1).

Finally, the boundary conditions can be verified for w and v. It is clear that $u(\mathbf{r}) \to 0$ as $|\mathbf{r}| \to \infty$ since $u = \Phi * H$, $\Phi(\mathbf{r}) \to 0$ as $|\mathbf{r}| \to \infty$, and H decays exponentially. Also, with (4.1) we get $w(\mathbf{r}) = \lambda^2\Phi(\mathbf{r}) - u(\mathbf{r})$ so that $w(\mathbf{r}) \to 0$ as $|\mathbf{r}| \to \infty$. Hence, from (4.9) it implies that v vanishes at infinity too. This completes the proof of Theorem 4.1. □

Remark 2: Conditions governing the existence of solutions in $\mathbb{R}^3$ involve weighted norms [1]. For example, let V denote the space of functions ψ such that both $\nabla\psi$ and $|\mathbf{r}|^{-1}\psi$ are square integrable. Then, for any $\rho \in V'$, (4.2) and (4.3) have solutions in V.

5. Analytical solutions of two nonlocal model problems. According to Theorem 4.1, we can solve the nonlocal model (2.1) for the electrostatic potential function Φ in the following three steps.

Step 1 Solve the Poisson-like equation (4.2) for w.

Step 2 Solve the Poisson equation (4.3) for v.

Step 3 Find the solution Φ of the nonlocal model (2.1) by the formula (4.1).

As an application, in this section, we use this procedure to find the analytical solutions of two nonlocal model problems: one is defined by (2.1) with ρ being a smooth function, and the other with $\rho(\mathbf{r}) = q\delta(\mathbf{r})$ (i.e., one charge q located at the origin). The one point charge problem deviates from our model in that ρ is singular, and so the problem no longer fits neatly in square-integrable Sobolev spaces. However, we will see that the splitting still works correctly. The smooth ρ is constructed artificially by us. Due to its simplicity, we will use it to validate the solution splitting formula and to study the computer performance of the program package.

5.1. A smooth problem. To construct a model problem with a smooth density function ρ and a known exact solution Φ, the solution u of (4.8) is set as

$$u(\mathbf{r}) = e^{-|\mathbf{r}|}|\mathbf{r}|^4, \quad \mathbf{r}\in\mathbb{R}^3.$$

Since it is a radial function, u can be regarded as a function of one variable r with $r = |\mathbf{r}|$ so that $u(\mathbf{r}) = u(r)$ and $\Delta u(\mathbf{r})$ can be calculated by using the formula

$$\Delta u(\mathbf{r}) = \frac{1}{r}\frac{\mathrm{d}^2}{\mathrm{d}r^2}(ru(r)).$$

Since $w(\mathbf{r}) = -\lambda^2 \Delta u(\mathbf{r})$, we find the solution w of (4.2) in the form

$$w(\mathbf{r}) = -\lambda^2 e^{-r}(r^4 - 10r^3 + 20r^2).$$

Applying the above w to (4.2) yields the density function ρ:

$$\begin{aligned}\rho(\mathbf{r}) = \ \epsilon_0 e^{-r}\Big[&\left(\epsilon_\infty - \frac{\epsilon_s}{\lambda}\right) r^4 + \left(\frac{10\epsilon_s}{\lambda^2} - 20\epsilon_\infty\right) r^3 \\ &+ \left(120\epsilon_\infty - \frac{20\epsilon_s}{\lambda^2}\right) r^2 - 240\epsilon_\infty r + 120\epsilon_\infty\Big].\end{aligned} \tag{5.1}$$

With (4.9), we then get the solution $v(\mathbf{r})$ of (4.3):

$$v(\mathbf{r}) = \lambda^2 e^{-r}\left[\left(\frac{\epsilon_s}{\lambda^2\epsilon_\infty} - 1\right) r^4 + 10r^3 - 20r^2\right].$$

Using the solution splitting formula (4.1), we obtain the exact solution of this model problem:

$$\Phi(\mathbf{r}) = e^{-r}\Big[\left(\frac{1}{\lambda^2} - 1\right) r^4 + 10r^3 - 20r^2\Big], \tag{5.2}$$

where $r = |\mathbf{r}|$, and $\mathbf{r} \in \mathbb{R}^3$.

5.2. One point charge problem. In this case, $w(\mathbf{r})$ is spherically symmetric. Thus, by using the spherical coordinates, (4.2) can be simplified as an ordinary differential equation:

$$-\frac{1}{r}\frac{\mathrm{d}^2}{\mathrm{d}r^2}\left(rw(r)\right) + \kappa^2 w(r) = 0, \quad r > 0, \tag{5.3}$$

where $\kappa = \frac{1}{\lambda}\sqrt{\frac{\epsilon_s}{\epsilon_\infty}}$, and $w(r) \to 0$ as $r \to \infty$. The general solution of this equation can be found as

$$w(r) = c_1\frac{e^{\kappa r}}{r} + c_2\frac{e^{-\kappa r}}{r},$$

where c_1 and c_2 are two constants. Since $\lim_{r\to\infty} w(r) = 0$, c_1 must be zero so that

$$w(r) = c_2\frac{e^{-\kappa r}}{r} \quad \forall r > 0. \tag{5.4}$$

To determine the value of c_2, we use the distributional form of (4.2):

$$-\int_{\mathbb{R}^3} w(\mathbf{r})\Delta\psi(\mathbf{r})\,\mathrm{d}\mathbf{r} + \frac{\epsilon_s}{\lambda^2\epsilon_\infty}\int_{\mathbb{R}^3} w(\mathbf{r})\psi(\mathbf{r})\,\mathrm{d}\mathbf{r} = \frac{\lambda^2 q}{\epsilon_0\epsilon_\infty}\psi(0) \quad \forall\psi \in C_0^\infty(\mathbb{R}^3), \tag{5.5}$$

where the definition of the Dirac-delta distribution,

$$\langle\delta, \psi\rangle = \psi(0) \quad \forall\psi \in C_0^\infty(\mathbb{R}^3),$$

has been used. From [27, Proposition, Page 36], it is known that for two given concentric balls, $B_\tau \subset B_\eta$ with $\eta > \tau > 0$, a particular test function, $\psi_\eta \in C_0^\infty(\mathbb{R}^3)$, can be constructed such that $\psi_\eta = 1$ on B_τ and 0 outside B_η while $\psi_\eta(\mathbf{r}) = \mu(\mathbf{r})$ for

$\tau \le |\mathbf{r}| \le \eta$, where μ is a smooth function satisfying that $\mu(\mathbf{s}) = 1$ and $\nabla\mu(\mathbf{s})\cdot\mathbf{n}(\mathbf{s}) = 0$ for $|\mathbf{s}| = \tau$, $\mu(\mathbf{s}) = \nabla\mu(\mathbf{s})\cdot\mathbf{n}(\mathbf{s}) = 0$ for $|\mathbf{s}| = \eta$, and $0 \le \mu \le 1$. For example, such a μ is given by

$$\mu(\mathbf{r}) = e^{1-\frac{(\eta-\tau)^2}{(\eta-\tau)^2-(|\mathbf{r}|-\tau)^2}} \quad \text{for } \tau \le |\mathbf{r}| \le \eta.$$

For this test function, it is clear that (5.5) becomes

$$-\int_{\tau\le|\mathbf{r}|\le\eta} w(\mathbf{r})\Delta\mu(\mathbf{r})\,\mathrm{d}\mathbf{r} + \frac{\epsilon_s}{\lambda^2\epsilon_\infty}\int_{B_\eta} w(\mathbf{r})\psi_\eta(\mathbf{r})\,\mathrm{d}\mathbf{r} = \frac{\lambda^2 q}{\epsilon_0\epsilon_\infty}. \tag{5.6}$$

By Green's identity, the definition of μ, and (4.2), the first term of the above equation can be simplified as

$$\int_{\tau\le|\mathbf{r}|\le\eta} w(\mathbf{r})\Delta\mu(\mathbf{r})\,\mathrm{d}\mathbf{r} = \frac{\epsilon_s}{\lambda^2\epsilon_\infty}\int_{\tau\le|\mathbf{r}|\le\eta} w(\mathbf{r})\mu(\mathbf{r})\,\mathrm{d}\mathbf{r} - \int_{|\mathbf{s}|=\tau}\nabla w(\mathbf{s})\cdot\mathbf{n}(\mathbf{s})\mathrm{d}\mathbf{s},$$

where $\mathbf{n}(\mathbf{s})$ is the unit normal vector pointing to the origin (i.e., $\mathbf{n}(\mathbf{s}) = -\mathbf{s}/\tau$). Obviously, the integral terms of $w\psi_\eta$ and $w\mu$ in the above two equations go to zero as η goes to zero, so we work only on the last term of the above equation.

Using the spherical coordinates (r, θ, ϕ) and (5.4), we obtain that

$$\begin{aligned}\int_{|\mathbf{s}|=\tau}\nabla w(\mathbf{s})\cdot\mathbf{n}(\mathbf{s})\mathrm{d}\mathbf{s} &= -\int_0^{2\pi}\int_0^{\pi}\left.\frac{\mathrm{d}w(r)}{\mathrm{d}r}\right|_{r=\tau}\tau^2\sin\phi\mathrm{d}\phi\mathrm{d}\theta \\ &= 4\pi(\kappa\tau+1)e^{-\kappa\tau}c_2 \to 4\pi c_2 \quad \text{as } \tau\to 0.\end{aligned}$$

Hence, letting $\eta \to 0$ in (5.6) yields

$$4\pi c_2 = \frac{\lambda^2 q}{\epsilon_0\epsilon_\infty},$$

and thus

$$c_2 = \frac{q\lambda^2}{4\pi\epsilon_\infty\epsilon_0}.$$

We next consider the solution of (4.3). By the spherical coordinates, we can formulate (4.3) as

$$-\frac{1}{r}\frac{\mathrm{d}^2}{\mathrm{d}r^2}(rv(r)) = 0, \quad r > 0,$$

and find its solution in the form

$$v(r) = \frac{q\lambda^2}{4\pi\epsilon_\infty\epsilon_0 r}, \tag{5.7}$$

where the fact that $v(r) \to 0$ as $r \to \infty$ has been used.

Applying both (5.4) and (5.7) to (4.1) immediately results in the solution

$$\Phi(r) = \frac{q}{4\pi\epsilon_s\epsilon_0\, r}\left(1 + \frac{\epsilon_s-\epsilon_\infty}{\epsilon_\infty}e^{-\kappa r}\right). \tag{5.8}$$

6. Fast finite element solver for the nonlocal model. In this section, we construct a fast finite element algorithm for solving the nonlocal dielectric model (2.1) according to the splitting formula of Theorem 4.1. Based on a finite element space $\mathcal{V}_h \subset H_0^1(\Omega)$, (4.2) and (4.3) are approximated as two finite element equations, respectively, as follows:

$$\int_\Omega \nabla w(\mathbf{r}) \cdot \nabla \psi(\mathbf{r})\, \mathrm{d}\mathbf{r} + \frac{\epsilon_s}{\lambda^2 \epsilon_\infty} \int_\Omega w(\mathbf{r})\psi(\mathbf{r}) d\mathbf{r} = \frac{\lambda^2}{\epsilon_0 \epsilon_\infty} \int_\Omega \rho(\mathbf{r})\psi(\mathbf{r}) d\mathbf{r} \quad \forall \psi \in \mathcal{V}_h$$

and

$$\int_\Omega \nabla v(\mathbf{r}) \cdot \nabla \psi(\mathbf{r})\, \mathrm{d}\mathbf{r} = \frac{\lambda^2}{\epsilon_0 \epsilon_\infty} \int_\Omega \rho(\mathbf{r})\psi(\mathbf{r}) d\mathbf{r} \quad \forall \psi \in \mathcal{V}_h,$$

where we have assumed that w and v are zero on the boundary of Ω.

By using $w(\mathbf{r}) = \sum_{j=1}^N w_j \varphi_j(\mathbf{r})$, and $v(\mathbf{r}) = \sum_{j=1}^N v_j \varphi_j(\mathbf{r})$, the above two variational forms can be formulated, respectively, as the following two linear systems:

$$\left(C_h + \frac{\epsilon_s}{\lambda^2 \epsilon_\infty} M_h \right) W_h = \frac{\lambda^2}{\epsilon_0 \epsilon_\infty} \rho_h \tag{6.1}$$

and

$$C_h V_h = \frac{\lambda^2}{\epsilon_0 \epsilon_\infty} \rho_h, \tag{6.2}$$

where W_h, V_h, and ρ_h denote the column vectors of order N with the ith entries being w_i, v_i, and $\int_\Omega \rho \varphi_i d\mathbf{r}$, respectively, C_h is a symmetric positive definite matrix of $N \times N$ with the ijth entry being $\int_\Omega \nabla \varphi_i(\mathbf{r}) \cdot \nabla \varphi_j(\mathbf{r})\, \mathrm{d}\mathbf{r}$, and M_h is the mass matrix with the ijth entry being $\int_\Omega \varphi_i(\mathbf{r}) \cdot \varphi_j(\mathbf{r})\, \mathrm{d}\mathbf{r}$.

As soon as W_h and V_h are found, the solution of the finite element equation (3.8) can be obtained by simply setting

$$\Phi_j = \frac{1}{\lambda^2 \epsilon_s} [(\epsilon_s - \epsilon_\infty) W_{h,j} + \epsilon_\infty V_{h,j}], \quad j = 1, 2, \ldots, N, \tag{6.3}$$

where $W_{h,j}$ and $V_{h,j}$ denote the jth component of W_h and V_h, respectively.

For clarity, we summarize our fast finite element algorithm for solving the nonlocal model (2.1) as follows:

1. Solve the linear system (6.1) for W_h by a fast iterative method.
2. Solve the linear system (6.2) for V_h by the same iterative method used in step 1.
3. Find the solution Φ_h of the nonlocal model (3.9) by using (6.3).

Note that there exist several fast iterative methods for solving Poisson and Poisson-like equations "optimally" in the sense that the computing amount is in a linear order of N (e.g., the multigrid method and the PCG method with a multigrid preconditioner [9, 14]). Hence, we claim that the nonlocal model (2.1) can be solved optimally by our fast finite element algorithm.

7. Numerical results. We programed our fast algorithm as a program package in Python based on the finite element library `DOLFIN` from the FEniCS project (see http://www.fenicsproject.org/). Because of the powerful functions of `DOLFIN`, both finite element equations (6.1) and (6.2) can be quickly formulated and solved. For test

purposes, we installed a FEniCS binary distribution for Mac OSX on our MacBook Pro, which contained `DOLFIN` version 0.9.10. The PCG algorithm with incomplete LU preconditioning from the `PETSc` library was used to solve each involved linear system. The default parameters of `PETSc` were employed for controlling convergence. All the numerical experiments were made on our MacBook Pro with one Intel Core I7 processor 2.66 GHz and 4 GB memory.

7.1. A smooth problem. Because the analytical solutions of (4.2) and (4.3) have been known in this model problem, we simply set Ω as the unit cube $[0,1] \times [0,1] \times [0,1]$ and construct a linear finite element approximation to (4.2) and (4.3), respectively, using the following inhomogeneous Dirichlet boundary conditions:

$$w(\mathbf{s}) = -\lambda^2 e^{-|\mathbf{s}|}(|\mathbf{s}|^4 - 10|\mathbf{s}|^3 + 20|\mathbf{s}|^2), \quad \mathbf{s} \in \partial\Omega,$$

and

$$v(\mathbf{s}) = \lambda^2 e^{-|\mathbf{s}|}\left[\left(\frac{\epsilon_s}{\lambda^2\epsilon_\infty} - 1\right)|\mathbf{s}|^4 + 10|\mathbf{s}|^3 - 20|\mathbf{s}|^2\right], \quad \mathbf{s} \in \partial\Omega.$$

In the numerical experiments, we used the `DOLFIN` function *UnitCube*$(2^k, 2^k, 2^k)$ to generate a uniform mesh, Ω_h, for $k = 2, 3, \ldots, 6$, where the grid size $h_k = 1/2^k$. Such a finite element approximation is equivalent to the finite difference approximation [10]. We set $\epsilon_\infty = 2$, $\epsilon_s = 80$, and $\lambda = 15$. We also calculated the relative and absolute errors E_r and E_a between the finite element solution $\Phi_h(\mathbf{r})$ and the analytical solution $\Phi(\mathbf{r})$ and estimated the convergence order p of the finite element method by using the following formulas:

$$E_r = \frac{1}{N_h}\sum_{j=1}^{N_h}\frac{|\Phi_j - \Phi(\mathbf{r}_j)|}{|\Phi(\mathbf{r}_j)|}, \quad E_a(h) = \sqrt{\int_\Omega |\Phi_h(\mathbf{r}) - \Phi(\mathbf{r})|^2 d\mathbf{r}} \tag{7.1}$$

and

$$p \approx p_k = \ln(|E_a(h_k)|/|E_a(h_{k-1})|)/\ln(h_k/h_{k-1}) \quad \text{for } k = 2, 3, \ldots, 6, \tag{7.2}$$

where $\Phi(\mathbf{r})$ has been given in (5.2), $\Phi_j = \Phi_h(\mathbf{r}_j)$ with $\mathbf{r}_j$ being the jth vertex of Ω_h, and N_h is the total number of interior vertices. The formula of p_k is obtained by assuming $E_a(h) = O(h^p)$. Since the linear finite element approximation was used in the calculation, p has been known to be 2 [10] so that p_k should approach 2 as h_k goes to zero if the calculation is correct. We calculated $E_a(h)$ using the `DOLFIN` function *errornorm*(Φ, Φ_h, norm_type='L2', degree=3) by a third order of finite element approximation. The computer CPU time consists of the solver time and the setup time, whose sum gives the total CPU time counted from the starting of mesh generation to the ending of finding the numerical solution. The solver time is the time spent on solving the two linear systems (6.1) and (6.2). The numerical results are reported in Table 7.1.

From Table 7.1 we can see that both E_r and E_a are reduced toward zero monotonically, and p_k approaches 2 as the grid size h decreases. These numerical results well validate our solution splitting formula and the corresponding program package. They also demonstrate the performance of our program package in terms of the computer CPU time. We note that the setup time is increased almost in a linear order of N_k, but this is not true for the solver time. We repeated these tests using an

TABLE 7.1

Performance of our program package for solving the nonlocal dielectric model (2.1) *with* $\rho(\mathbf{r})$ *being given in* (5.1). *Here* E_r *and* E_a *are defined in* (7.1), p_k *is an estimation of finite element error order defined in* (7.2), *and* N_{h_k} *is the number of unknowns.*

h_k	N_{h_k}	Relative error E_r	Absolute error E_a	Error order p_k	CPU time (sec.) Setup	Solver
1/4	27	1.34×10^{-2}	9.41×10^{-2}	1.6892	0.0229	0.0030
1/8	343	2.80×10^{-3}	2.54×10^{-2}	1.8887	0.08910	0.0075
1/16	3375	6.16×10^{-4}	6.48×10^{-3}	1.9698	0.5554	0.0672
1/32	29791	1.43×10^{-4}	1.63×10^{-3}	1.9924	4.6735	0.7731
1/64	250047	3.43×10^{-5}	4.08×10^{-4}	1.9981	36.5015	7.6281

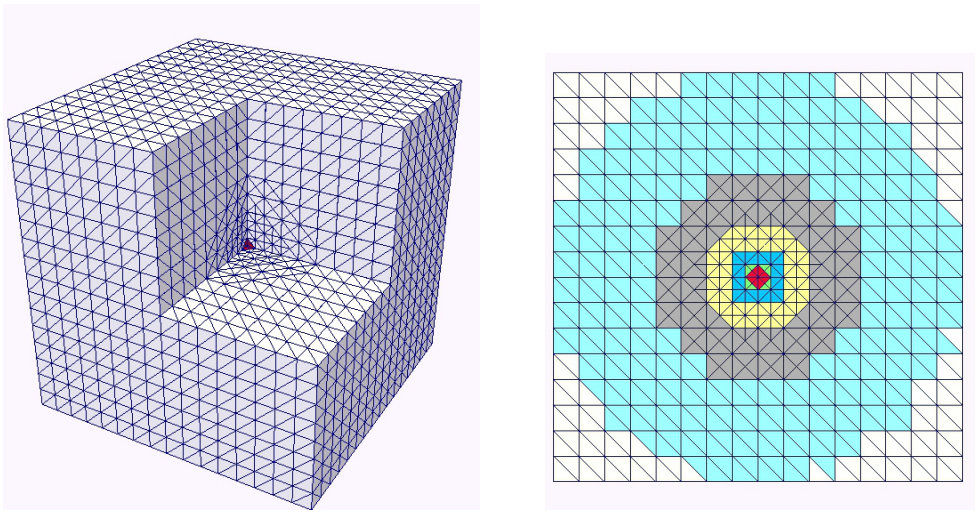

FIG. 7.1. *A mesh partition of the unit cubic domain* Ω *with one octant being removed for displaying the mesh structure around the point charge* q *in the center, along with a cross section of the mesh on the xy-plane. Each triangle represents the projection of a tetrahedron, which is marked in five colors (cyan, gray, yellow, blue, and green) to indicate areas where tetrahedra were generated in the five steps of refinement. The triangles from the initial mesh are in white. The support domain* ω_h *is marked out in red, whose volume is* 6.10×10^{-5}. *Color is available only in the online version*

algebraic multigrid preconditioner, called *amg_hypre*, from `PETSc`. We found that the total number of PCG iterations was sharply reduced to a small number around 6 for all five test problems with N_k from 27 to 250,047, which confirms that the PCG using *amg_hypre* has a small rate of convergence independent of N_k. However, the solver time was increased a lot. For example, in solving (6.2) with $h_k = 1/64$, the solver time was increased from 7.6281 to 12.671 seconds in spite of the total number of PCG iterations being reduced from 95 to 6. It appears from our data that our problem size is not large enough for the efficiency of multigrid preconditioner *amg_hypre* to be needed. Indeed our setup times dominate our solve times.

7.2. One point charge model problem. As a further verification, we also solved the one point charge problem as defined by the nonlocal model (2.1) with $\rho(\mathbf{r}) = q\delta(\mathbf{r})$. This test problem provides a significant challenge due to the strong singularity.

In our numerical tests, the Dirac-delta distribution δ is simply approximated by

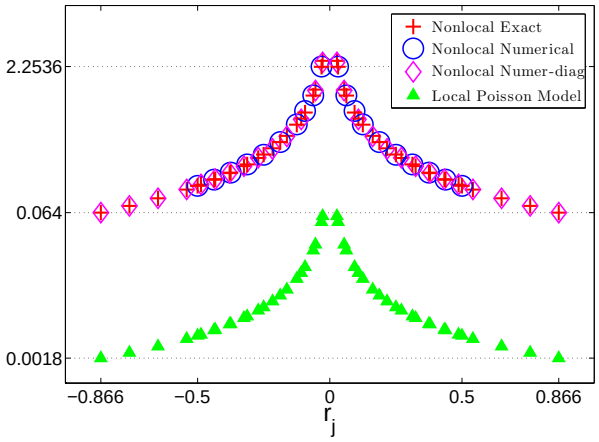

FIG. 7.2. *Comparisons of the numerical solutions with the analytical solutions for the local and nonlocal one point charge problems at the mesh points* $\mathbf{r}_j$ *lying on both the* x*-axis line and the diagonal line defined by* $x = y = z$*. Here* $q = 1e$*,* $\lambda = 15$*,* $\epsilon_\infty = 1.8$*,* $\epsilon_s = 80$*, and the mesh for calculating the numerical solution is shown in Figure 7.1.*

a discrete Dirac-delta function, δ_h, defined as follows:

$$\delta_h(\mathbf{r}) = \begin{cases} \frac{1}{\text{volume of } \omega_h} & \text{for } \mathbf{r} \in \omega_h, \\ 0 & \text{otherwise,} \end{cases}$$

where ω_h denotes the support of a finite element base function at the origin point $(0, 0, 0)$. In particular, ω_h is the tetrahedron element that contains the origin if the origin is not a mesh grid point. For simplicity, the domain Ω is set as the unit cube. An initial mesh was generated by calling the `DOLFIN` function *Box*(−0.5, −0.5, −0.5, 0.5, 0.5, 0.5, 16, 16, 16). To improve the accuracy of δ_h, it was then refined around the origin by using a simple local mesh refinement scheme. That is, a tetrahedron element of the mesh is marked as the one to be refined if the distance of its center point to the origin is less than $1/2^k$. According to the marked tetrahedron information, which is stored in a bool array called *cell_markers*, the mesh is then refined by calling the `DOLFIN` function *refine*(*mesh, cell_markers*). This mesh refinement was done repeatedly for $k = 1, 2, 3, 4, 5$ in our numerical tests.

Figure 7.1 displays the mesh that we used in solving the one point charge problem, along with a cross section of the mesh on the xy-plane to clearly show the process of mesh refinement. In the cross section figure of Figure 7.1, each triangle represents the projection of a tetrahedron element onto the xy-plane, and the different colors(available only in the online version) indicate areas where tetrahedra were generated in different steps of refinement: white for the initial mesh while cyan, gray, yellow, blue, and green for the first to fifth steps of refinements, respectively. The support domain ω_h is marked out in red. Due to the view angle of projection, tetrahedra from different color areas may have the same triangular projection on the xy-plane. For example, the cyan triangles are the projection of the tetrahedra refined in the first step of refinement; they have the same shape as the white triangles, which are the projection of the tetrahedra from the initial mesh. This mesh has 8,399 vertices and 43,908 tetrahedra. The smallest and largest grid sizes are 0.0349 and 0.1082, respectively. The origin was a vertex of the mesh, ω_h consisted of 48 tetrahedra, and

the volume of ω_h was 6.10×10^{-5}. The boundary condition was chosen to be Dirichlet with the values equal to the analytical solution on the surface of the unit cube.

The average relative error E_r defined in (7.1) was found to be 3.4195×10^{-3} for this one point charge problem. Furthermore, Figure 7.2 compares the numerical and analytical solutions lying on the x-axis line and the diagonal line defined by $x = y = z$, where one might not expect as good of results. From the figures we see excellent agreement in both cases. Thus, the calculations appear to be very robust as well as accurate and efficient. This confirms our new solution splitting formula further.

As a comparison, the analytical solution of the classic Poisson dielectric model for the case of one point charge, $\Phi(\mathbf{r}) = q/(4\pi\epsilon_s\epsilon_0|\mathbf{r}|)$ for $\mathbf{r} \neq (0,0,0)$, was also plotted in Figure 7.2. From this figure we see that the nonlocal solution is very different from the corresponding local Poisson solution.

Appendix. **Free energy calculation and analytical solution of a nonlocal Born ion model** In this appendix, we derive the analytical solution of a nonlocal Born ion model and then use it to calculate the free energy of solvation. The nonlocal Born ion model is defined as follows:

$$\begin{cases} \Delta\Phi_b(\mathbf{r}) = 0, & |\mathbf{r}| < a, \\ \epsilon_\infty \Delta\Phi_s(\mathbf{r}) + \frac{\epsilon_s - \epsilon_\infty}{\lambda^2}\nabla\cdot\hat{v}(\mathbf{r}) = 0, & |\mathbf{r}| > a, \\ \Phi_b(\mathbf{s}) = \Phi_s(\mathbf{s}), & |\mathbf{s}| = a, \\ \left(\nabla\Phi_b(\mathbf{s}) - \epsilon_\infty\nabla\Phi_s(\mathbf{s}) - \frac{\epsilon_s-\epsilon_\infty}{\lambda^2}\hat{v}(\mathbf{s})\right)\cdot\mathbf{n} = \frac{q}{4\pi\epsilon_0 a^2}, & |\mathbf{s}| = a, \end{cases} \tag{.3}$$

where Φ_b and Φ_s denote the restrictions of Φ onto the ball range $|\mathbf{r}| < a$ and the water solvent range $|\mathbf{r}| > a$, respectively, $\Phi_s(\mathbf{r}) \to 0$ as $|\mathbf{r}| \to \infty$, and

$$\hat{v}(\mathbf{r}) = \int_{|\mathbf{r}|>a} H(\mathbf{r}-\mathbf{r}')\nabla_{\mathbf{r}'}\Phi_s(\mathbf{r}')\,d\mathbf{r}'.$$

Here an ion with charge q at the origin has been modeled as a ball with radius a and dielectric parameter ϵ_0 (i.e., the interior of the ball is in vacuum). Since charge q is uniformly spread over the spherical surface, the charge density function $\rho(\mathbf{r})$ of this Born model can be expressed as

$$\rho(\mathbf{r}) = \frac{q}{4\pi a^2}\delta(|\mathbf{r}| - a), \quad \mathbf{r} \in \mathbb{R}^3. \tag{.4}$$

To find the analytical solution of the above nonlocal Born model, we extend $\Phi_s(\mathbf{r})$ continuously into the ball by setting

$$\Phi_s(\mathbf{r}) = \Phi_s(\mathbf{s}) \quad \text{for } |\mathbf{r}| < a \text{ with } |\mathbf{s}| = a. \tag{.5}$$

In this way, we express $\hat{v}$ in the convolution form

$$\hat{v}(\mathbf{r}) = \int_{\mathbb{R}^3} H(\mathbf{r}-\mathbf{r}')\nabla_{\mathbf{r}'}\Phi_s(\mathbf{r}')\,d\mathbf{r}' = (\nabla\Phi_s * H)(\mathbf{r}).$$

Similar to what is done in Section 2.2, we formulate the second equation of (.3) as

$$\epsilon_\infty\Delta\Phi_s(\mathbf{r}) - \frac{\epsilon_s-\epsilon_\infty}{\lambda^2}\Phi_s(\mathbf{r}) + \frac{\epsilon_s-\epsilon_\infty}{\lambda^4}w(\mathbf{r}) = 0, \quad |\mathbf{r}| > a, \tag{.6}$$

where $w(\mathbf{r}) = (H * \Phi_s)(\mathbf{r})$, and w can be found to satisfy the equation

$$-\Delta w(\mathbf{r}) + \frac{1}{\lambda^2} w(\mathbf{r}) - \Phi_s(\mathbf{r}) = 0, \quad \mathbf{r} \in \mathbb{R}^3.$$

We then set $w_b = w(\mathbf{r})$ for $|\mathbf{r}| < a$ and $w_s = w(\mathbf{r})$ for $|\mathbf{r}| > a$ and transform the nonlocal Born model (.3) as an interface system:

$$\begin{cases} \Delta \Phi_b(\mathbf{r}) = 0, \\ -\Delta w_b(\mathbf{r}) + \frac{1}{\lambda^2} w_b(\mathbf{r}) - \Phi_s(\mathbf{r}) = 0, \qquad |\mathbf{r}| < a, \end{cases} \tag{.7}$$

and

$$\begin{cases} \epsilon_\infty \Delta \Phi_s(\mathbf{r}) - \frac{\epsilon_s - \epsilon_\infty}{\lambda^2} \Phi_s(\mathbf{r}) + \frac{\epsilon_s - \epsilon_\infty}{\lambda^4} w_s(\mathbf{r}) = 0, \\ -\Delta w_s(\mathbf{r}) + \frac{1}{\lambda^2} w_s(\mathbf{r}) - \Phi_s(\mathbf{r}) = 0, \qquad |\mathbf{r}| > a, \end{cases} \tag{.8}$$

where the interface conditions are given by

$$\Phi_b(\mathbf{s}) = \Phi_s(\mathbf{s}), \quad w_b(\mathbf{s}) = w_s(\mathbf{s}), \quad \frac{\partial w_b(\mathbf{s})}{\partial \mathbf{n}(\mathbf{s})} = \frac{\partial w_s(\mathbf{s})}{\partial \mathbf{n}(\mathbf{s})} \quad \text{for } |\mathbf{s}| = a$$

and

$$\frac{\partial \Phi_b(\mathbf{s})}{\partial \mathbf{n}(\mathbf{s})} - \epsilon_\infty \frac{\partial \Phi_s(\mathbf{s})}{\partial \mathbf{n}(\mathbf{s})} - \frac{\epsilon_s - \epsilon_\infty}{\lambda^2} \frac{\partial w_s(\mathbf{s})}{\partial \mathbf{n}(\mathbf{s})} = \frac{q}{4\pi\epsilon_0 a^2} \quad \text{for } |\mathbf{s}| = a.$$

Since Φ, H, and w are radial functions, by spherical coordinates, the above interface system can be transformed as a system of ordinary differential equations:

$$\begin{cases} \frac{\mathrm{d}^2}{\mathrm{d}r^2}\left(r\Phi_b(r)\right) = 0, \\ -\frac{\mathrm{d}^2}{\mathrm{d}r^2}\left(r w_b(r)\right) + \frac{1}{\lambda^2} r w_b(r) - r\Phi_s(a) = 0 \quad \text{for } \ 0 < r < a \end{cases} \tag{.9}$$

and

$$\begin{cases} -\frac{\mathrm{d}^2}{\mathrm{d}r^2}\left(r\Phi_s(r)\right) + \frac{(\epsilon_s - \epsilon_\infty)}{\epsilon_\infty \lambda^2}\left[r\Phi_s(r) - \frac{1}{\lambda^2} r w_s(r)\right] = 0, \\ -\frac{\mathrm{d}^2}{\mathrm{d}r^2}\left(r w_s(r)\right) + \frac{1}{\lambda^2} r w_s(r) - r\Phi_s(r) = 0 \quad \text{for } \ a < r < \infty, \end{cases} \tag{.10}$$

where the boundary and interface conditions are given by

$$w_s(r) \to 0 \quad \text{and} \quad \Phi_s(r) \to 0 \quad \text{as } r \to \infty, \quad \Phi_b(a) = \Phi_s(a), \quad w_b(a) = w_s(a),$$

$$w_b'(a) = w_s'(a), \quad \text{and} \quad \Phi_b'(a) - \epsilon_\infty \Phi_s'(a) - \frac{\epsilon_s - \epsilon_\infty}{\lambda^2} w_s'(a) = \frac{q}{4\pi\epsilon_0 a^2}.$$

Here the extension (.5) of Φ_s has been used in the second equation of (.9). Additionally, from the continuity of w_b and Φ_b it implies that

$$\lim_{r \to 0} r w_b(r) = 0 \quad \text{and} \quad \lim_{r \to 0} r\Phi_b(r) = 0.$$

Solving the system of (.9) and (.10) immediately results in the analytical solution of the nonlocal Born model (.3) in the form

$$\Phi(\mathbf{r}) = \begin{cases} \dfrac{q}{4\pi\epsilon_0\epsilon_s} \dfrac{\sqrt{\epsilon_\infty \epsilon_s} + \epsilon_s \coth(a/\lambda)}{[\lambda(\epsilon_\infty - \epsilon_s) + a(\sqrt{\epsilon_\infty \epsilon_s} + \epsilon_s \coth(a/\lambda))]}, & |\mathbf{r}| \le a, \\ \dfrac{q}{4\pi\epsilon_0\epsilon_s |\mathbf{r}|} \left[1 + \dfrac{\lambda(\epsilon_s - \epsilon_\infty) e^{\kappa(a - |\mathbf{r}|)}}{\lambda(\epsilon_\infty - \epsilon_s) + a(\sqrt{\epsilon_\infty \epsilon_s} + \epsilon_s \coth \frac{a}{\lambda})}\right], & |\mathbf{r}| > a, \end{cases} \tag{.11}$$

where $\coth x = (e^{2x}+1)/(e^{2x}-1)$ is the hyperbolic cotangent function.

Two local Born models—one in the vacuum and the other in water—can be generated from the nonlocal Born model (.3) by setting $\epsilon_s = \epsilon_\infty = 1$ and $\epsilon_s = \epsilon_\infty$, respectively. Thus, their analytical solutions, Φ_v and Φ_w, can be directly followed from (.11) as follows:

$$\Phi_v = \begin{cases} \dfrac{q}{4\pi\epsilon_0 a}, & |\mathbf{r}| \le a, \\ \dfrac{q}{4\pi\epsilon_0|\mathbf{r}|}, & |\mathbf{r}| > a, \end{cases} \quad \text{and} \quad \Phi_w = \begin{cases} \dfrac{q}{4\pi\epsilon_0\epsilon_s a}, & |\mathbf{r}| \le a, \\ \dfrac{q}{4\pi\epsilon_0\epsilon_s|\mathbf{r}|}, & |\mathbf{r}| > a. \end{cases} \tag{.12}$$

We are now in the position to estimate the free energy of solvation of the nonlocal Born model problem. Set $\sigma(r) = r^2[\Phi(r) - \Phi_v(r)]$ for $r = |\mathbf{r}|$. Using (.4), (.11), (.12), and spherical coordinates, we estimate the free energy ΔG as follows:

$$\begin{aligned} \Delta G &\approx \frac{\mathcal{N}_a}{1000}\frac{1}{2}\int_{\mathbb{R}^3}\rho(\mathbf{r})[\Phi(\mathbf{r}) - \Phi_v(\mathbf{r})]\mathrm{d}\mathbf{r} \\ &= \frac{\mathcal{N}_a}{1000}\frac{1}{2}\int_0^\infty\int_0^{2\pi}\int_0^\pi \rho(r)[\Phi(r) - \Phi_v(r)]r^2\sin\phi\mathrm{d}\phi\mathrm{d}\theta\mathrm{d}r \\ &= \frac{\mathcal{N}_a}{1000}2\pi\int_0^\infty \rho(r)\sigma(r)\mathrm{d}r = \frac{\mathcal{N}_a}{1000}2\pi\left\langle\frac{q}{4\pi a^2}\delta_a, \sigma\right\rangle \\ &= \frac{\mathcal{N}_a}{1000}\frac{q}{2a^2}\sigma(a) = \frac{\mathcal{N}_a}{1000}\frac{q}{2}[\Phi(a) - \Phi_v(a)] \\ &= \frac{\mathcal{N}_a}{1000}\frac{q}{2}\left[\frac{q}{4\pi\epsilon_0\epsilon_s}\frac{\sqrt{\epsilon_\infty\epsilon_s} + \epsilon_s\coth\frac{a}{\lambda}}{a\sqrt{\epsilon_\infty\epsilon_s} + \lambda(\epsilon_\infty - \epsilon_s) + a\epsilon_s\coth\frac{a}{\lambda}} - \frac{q}{4\pi\epsilon_0 a}\right] \\ &= \frac{\mathcal{N}_a}{1000}\frac{q^2}{8\pi\epsilon_0\epsilon_s a}\left[\frac{\sqrt{\frac{\epsilon_\infty}{\epsilon_s}} + \coth\frac{a}{\lambda}}{\sqrt{\frac{\epsilon_\infty}{\epsilon_s}} + \frac{\lambda}{a}(\frac{\epsilon_\infty}{\epsilon_s} - 1) + \coth\frac{a}{\lambda}} - \epsilon_s\right], \end{aligned} \tag{.13}$$

where we have expressed $\rho(r)$ as distribution $\rho = \frac{q}{4\pi a^2}\delta_a$.

Finally, by setting $\epsilon_\infty = \epsilon_s$, the free energy ΔG^{local} of the local Born model in water solvent can be followed directly from (.13):

$$\Delta G^{local} \approx \frac{\mathcal{N}_a}{1000}\frac{q^2}{8\pi\epsilon_0\epsilon_s a}\Big(1 - \epsilon_s\Big). \tag{.14}$$

REFERENCES

[1] C. Amrouche, V. Girault, and J. Giroire, *Weighted Sobolev spaces for Laplace's equation in R^n*, J. Math. Pures Appliqu. (9), 73 (1994), pp. 579–606.

[2] S. Balay, J. Brown, K. Buschelman, V. Eijkhout, W.D. Gropp, D. Kaushik, M.G. Knepley, L.C. McInnes, B.F. Smith, and H. Zhang, *PETSc users manual*, Technical report ANL-95/11 - Revision 3.1, Argonne National Laboratory, Lemont, IL, 2010.

[3] S. Balay, J. Brown, K. Buschelman, W.D. Gropp, D. Kaushik, M.G. Knepley, L.C. McInnes, B.F. Smith, and H. Zhang, *PETSc*, http://www.mcs.anl.gov/petsc (2011).

[4] M.V. Basilevsky and G.N. Chuev, *Nonlocal solvation theories*, in Continuum Solvation Models in Chemical Physics: From Theory to Applications, B. Mennucci and R. Cammi, eds., Wiley, 2008, pp. 94–109.

[5] M.V. Basilevsky and D.F. Parsons, *An advanced continuum medium model for treating solvation effects: Nonlocal electrostatics with a cavity*, J. Chem. Phys., 105(1996), pp.3734–3746.

[6] M.V. Basilevsky and D.F. Parsons, *Nonlocal continuum solvation model with exponential susceptibility kernels*, J. Chem. Phys., 108 (1998), pp. 9107–9113.

[7] M.V. Basilevsky and D.F. Parsons, *Nonlocal continuum solvation model with oscillating susceptibility kernels: A nonrigid cavity model*, J. Chem. Phys., 108 (1998) pp. 9114–9123.
[8] P.A. Bopp, A.A. Kornyshev, and G. Sutmann, *Static nonlocal dielectric function of liquid water*, Phys. Rev. Lett., 76 (1996), pp. 1280–1283.
[9] J.H. Bramble, J.E. Pasciak, and J. Xu, *Parallel multilevel preconditioners*, Math. Comp., 55(1990), pp. 1–22.
[10] S.C. Brenner and L.R. Scott, *The Mathematical Theory of Finite Element Methods*, volume 15 of *Texts Appl. Math. 15,* Springer-Verlag, New York, 2002.
[11] J. Dai, I. Tsukerman, A. Rubinstein, and S. Sherman, *New computational models for electrostatics of macromolecules in solvents*, IEEE Transactions on Magn., 43(2007), pp. 1217–1220.
[12] T.A. Davis, *Algorithm 832: UMFPACK V4.3—an unsymmetric-pattern multifrontal method*, ACM Trans. Math. Software, 30 (2004), pp. 196–199.
[13] R.R. Dogonadze, E. Kálmán, A.A. Kornyshev, and J. Ulstrup, *The Chemical Physics of Solvation, Part A: Theory of Solvation*, Elsevier Science Ltd., Oxford, UK, 1985.
[14] W. Hackbusch, *Multigrid Methods and Applications*, Springer Ser. in Comput. Math., Springer Verlag, Berlin, 1985.
[15] J. B. Hasted, *Aqueous Dielectrics*, Chapman and Hall, London, 1974.
[16] M.A. Heroux, R.A. Bartlett, V.E. Howle, R.J. Hoekstra, J.J. Hu, T.G. Kolda, R.B. Lehoucq, K.R. Long, R.P. Pawlowski, E.T. Phipps, A.G. Salinger, H.K. Thornquist, R.S. Tuminaro, J.M. Willenbring, A. Williams, and K.S. Stanley, *An overview of the Trilinos project*, ACM Trans. Math. Software, 31 (2005), pp. 397–423.
[17] Andreas Hildebrandt, *Biomolecules in a Structured Solvent: A Novel Formulation of Nonlocal Electrostatics and Its Numerical Solution*, PhD thesis, Saarlandes University, Saarbrücken, Germany, 2005.
[18] A. Hildebrandt, R. Blossey, S. Rjasanow, O. Kohlbacher, and H.-P. Lenhof, *Novel formulation of nonlocal electrostatics*, Phys. Rev. Lett., 93 (2004), 108104.
[19] B. Honig and A. Nicholls, *Classical electrostatics in biology and chemistry*, Science, 268 (1995), pp. 1144–1149.
[20] A.A. Kornyshev and G. Sutmann, *Nonlocal dielectric saturation in liquid water*, Phys. Rev. Lett., 79 (1997), pp. 3435–3438.
[21] A.A. Kornyshev and G. Sutmann, *Nonlocal dielectric function of water: How strong are the effects of intramolecular charge form factors?* J. Mol. Liq., 82 (1999), pp. 151–160.
[22] A. Logg and G.N. Wells, *DOLFIN: Automated finite element computing*, ACM Trans. Math. Software, 37 (2010), 20.
[23] B.Z. Lu, Y.C. Zhou, M.J. Holst, and J.A. McCammon, *Recent progress in numerical methods for the Poisson-Boltzmann equation in biophysical applications*, Commun. Comput. Phys., 3(2008), pp. 973–1009.
[24] Yizhak Marcus, *Ion Solvation,* Wiley, New York, 1985.
[25] A. Rubinstein, R.F. Sabirianov, W.N. Mei, F. Namavar, and A. Khoynezhad, *Effect of the ordered interfacial water layer in protein complex formation: A nonlocal electrostatic approach*, Physical Rev. E, (3), 82 (2010), 021915.
[26] A. Rubinstein and S. Sherman, *Influence of the solvent structure on the electrostatic interactions in proteins*, Biophys. J., 87 (2004), pp. 1544–1557.
[27] W. Rudin, *Functional Analysis, 2nd ed.*, Internat. Ser. in Pure Appl. Math. McGraw-Hill, New York, 1991.
[28] L.R. Scott, M. Boland, K. Rogale, and A. Fernández, *Continuum equations for dielectric response to macro-molecular assemblies at the nano scale*, J. Phys. A, 37 (2004), pp. 9791–9803.
[29] S. Weggler, V. Rutka, and A. Hildebrandt, *A new numerical method for nonlocal electrostatics in biomolecular simulations*, J. of Comput. Phys., 229 (2101), pp. 4059–4074.
[30] G.J. Wilson, R.K. Chan, D.W. Davidson, and E. Whalley, *Dielectric properties of ices II, III, V, and VI,* J. Chem. Phys., 43 (1965), 2384.
[31] H. Yada, M. Nagai, and K. Tanaka, *The intermolecular stretching vibration mode in water isotopes investigated with broadband terahertz time-domain spectroscopy,* Chem, Phys. Lett., 473 (2009), pp. 279–283.